The sticking probability for H-2 on some transition metals at a hydrogen pressure of 1 bar

Johansson, Martin; Lytken, Ole; Chorkendorff, Ib

Published in:
Journal of Chemical Physics

Link to article, DOI:
10.1063/1.2825296

Publication date:
2008

Document Version
Publisher's PDF, also known as Version of record

The sticking probability for H_2 on some transition metals at a hydrogen pressure of 1 bar

M. Johansson,[a] O. Lytken, and I. Chorkendorff
Danish National Research Foundation's Center for Individual Nanoparticle Functionality (CINF) and Nano DTU, Department of Physics, Technical University of Denmark, DK-2800 Kgs. Lyngby, Denmark

(Received 19 September 2007; accepted 20 November 2007; published online 16 January 2008)

The sticking probability for hydrogen on films of Co, Ni, Cu, Ru, Rh, Pd, Ir, and Pt supported on graphite has been measured at a hydrogen pressure of 1 bar in the temperature range 40–200 °C. The sticking probability is found to increase in the order Ni, Co, Ir, Pd, Pt, Rh, and Ru at temperatures below 150 °C, whereas at higher temperatures, the sticking probability for Pd is higher than for Pt. The sticking probability for Cu is below the detection limit of the measurement. The measured sticking probabilities are slightly lower than those obtained at high hydrogen coverage under ultrahigh vacuum conditions. This could be a consequence of the higher hydrogen pressure used here. The apparent desorption energies extracted from the steady-state desorption rate are found to agree reasonably well with published values for the heat of adsorption at high coverage. However, the sticking probability is not related in a simple way to published values for the heat of adsorption at low coverage, with Ru and Rh giving exceptionally high values for the sticking probability. It is suggested that this is due to the presence of adsorption sites with very low desorption energy on Ru and Rh. © *2008 American Institute of Physics*. [DOI: 10.1063/1.2825296]

I. INTRODUCTION

The present strong interest in fuel cells and hydrogen storage motivates fundamental studies of hydrogen splitting on transition metals at realistic hydrogen pressures. In addition, the interaction of hydrogen with transition metals is of interest with respect to many industrially important catalytic reactions. Recent progress in theory has made it possible to calculate trends in the hydrogen binding energy between metals and metal alloys.[1] Such calculations have been employed to predict trends in the performance of real catalysts. An example is the successful attempt to relate the exchange current for the hydrogen evolution reaction with calculated binding energies for hydrogen on metals.[2] In this context, quantitative measurements of rates made under well controlled conditions should be a useful test of the theoretical predictions. Ultimately, insights into the mechanisms of hydrogen adsorption/desorption on metal surfaces at high pressure will hopefully result in metal alloy catalysts with improved performance.

The interaction of hydrogen with metal surfaces has been reviewed by Christmann.[3] Most of this work was performed on single crystal surfaces under ultrahigh vacuum (UHV) conditions, where high hydrogen coverage is achieved by dosing gas at low surface temperature. A variety of methods has been used to measure the hydrogen coverage. These include changes in the work function,[4,5] nuclear microanalysis,[6] low energy recoil scattering,[7] molecular beam techniques,[8,9] and integration of data from thermally programed desorption (TPD),[10] where the references given are examples of work on the metals studied here.

The sticking probability is either measured directly with molecular beam techniques or extracted from TPD data in experiments with adsorption of isotropic gas. In general, the sticking probability is found to drop with hydrogen coverage, and to be higher on surfaces with defects or steps.[3,11]

The heat of adsorption for hydrogen can be derived from measurements of the equilibrium coverage as a function of temperature and pressure; examples of the use of this method are given in Refs. 4 and 5. The activation energy for desorption is extracted from TPD data and molecular beam experiments, see examples in Refs. 10 and 12. In general, the heat of adsorption and the desorption energy are reported to drop with increasing coverage.

An investigation of hydrogen splitting at 1 bar hydrogen pressure on Ni, Pd, and Pt has been published previously, along with a detailed description of the method used.[13] The study was carried out on thin films supported on graphite, since this is the substrate used for the anode catalyst in the proton exchange membrane (PEM) fuel cell. In short, the dissociative sticking probability of hydrogen at 1 bar is extracted from measurements of the H–D exchange rate under the assumption that the sticking probabilities are equal for H_2, HD, and D_2. A simple model for the surface reactions is used to relate the sticking probabilities to the net H–D exchange rate. The exchange rate is extracted from measurements of the local gas composition close to the surface. A well defined geometry enables the use of computational fluid dynamics calculations to find the relation between the exchange rate and the gas composition at the point of measurement. Once the sticking probability is known, the adsorption rate for pure H_2 can be calculated, and, since the rates of adsorption and desorption have to be equal in steady state, this also yields the steady-state desorption rate.

In this study, the investigation is expanded to the metals

[a]Electronic mail: marjo@fysik.dtu.dk.

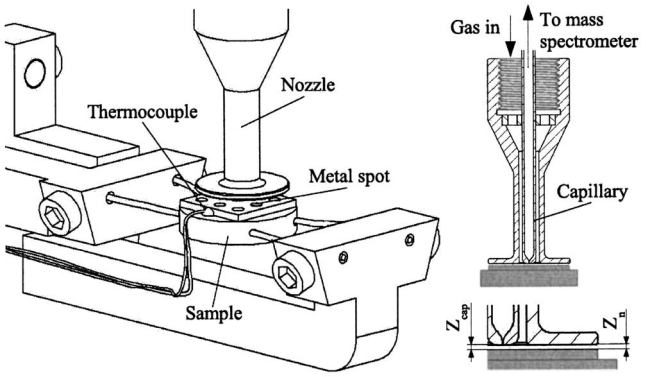

FIG. 1. The principles of the high pressure experiment. The left figure shows the gas sampling device positioned over a sample with metal spots. The right part of the figure shows a section of the gas sampling device. The distance between the tip of the capillary, where the leak is situated, and the sample surface, Z_{cap}, is 0.2 mm, as is the distance between the nozzle and the sample surface, Z_n.

Cu, Co, Ir, Rh, and Ru. It might have been expected that the metals with the highest binding energy for hydrogen would have the highest hydrogen coverage at a certain temperature, and thus the lowest sticking probability. Surprisingly, the sticking probability is highest for Ru, which is known to bind hydrogen the strongest of the investigated metals. Furthermore, the apparent activation energy[14] for desorption of hydrogen from Rh and Ru is found to be merely a few kJ/mole H_2. The anomalously high desorption rate for Rh and Ru is ascribed to the presence of adsorption states with low adsorption energy, which are populated at high coverage. Hydrogen splitting/association on these metals at 1 bar is thus an example of a system where the density of adsorption states as a function of adsorption energy determines the reactivity, rather than the adsorption energy at low coverage.

II. EXPERIMENTAL DETAILS

The apparatus used in this study consists of an ultrahigh vacuum chamber equipped with a high pressure cell and has been described in a previous publication.[15] In the vacuum chamber, model catalysts in the form of circular spots are produced by electron beam evaporation of metals onto a substrate. The vacuum chamber is also used for characterization of the spots with Auger electron spectroscopy (AES) and scanning electron microscopy (SEM). In the high pressure cell, the individual catalytic activity of the metal spots is tested by measuring the local gas composition over the catalytic surface. Figure 1 shows the principles of the high pressure experiment. The gas is sampled with a quartz capillary leak, made from a 1 mm o.d. quartz tube, and analyzed with mass spectrometry. The quartz tube is mounted concentrically in the gas inlet nozzle, see Fig. 1, and gas is blown toward the sample surface through the annulus between the capillary and the nozzle. The entire gas sampling device can be moved in three dimensions over the sample. When the sampling device is positioned over the center of one of the spots, the gas flow will prevent products formed on the other spots from influencing the measurement.[16] The substrate is a highly ordered pyrolytic graphite (HOPG) sample 7×7 mm^2 which is glued (Graphi-Bond 669, Aremco Products) onto a graphite disk, 10 mm in diameter and about 2 mm in thickness. The graphite disk is mounted on two tungsten wires, which are used for heating. The sample temperature is measured with a thermocouple glued onto the graphite disk at the edge of the HOPG sample, see Fig. 1. The gases used are N60 (99.9999%) H_2 and 99.8% D_2 (main contaminant HD) which are additionally purified by guard catalysts (Haldor Topsoe MK 121, activated in hydrogen at 240 °C). In order to avoid contamination by sulfur, the high pressure cell was cleaned by flowing hydrogen through it at 1 bar for 48 h during bakeout at 150 °C.

Some of the experimental procedures have been described in detail in a previous publication.[13] In short, the HOPG sample is cleaned by Ar sputtering for several hours between experiments, followed by heating to 800 °C for 20 min to desorb any remaining Ar from the sample. The metal spots are evaporated with the substrate at room temperature, with typical evaporation rates of 5–10 Å/min. The thickness of the spots is 50 Å and the diameter is 1 mm. The spot thickness is determined by calibrating the evaporation rate with the help of a quartz crystal microbalance. After evaporation, the sample is kept at 150 °C. The cleanliness of the spots is checked with AES before the sample is moved to the high pressure cell. Auger spectra are obtained with 3 kV primary energy while scanning the beam over a part of the spot area, typically the analyzed area is 0.5×0.5 mm^2. The electron beam has a width of more than 1 μm and the beam current is on the order of 2 μA. There were no visible cracks in the metal films, as judged by SEM. However, the resolution of the SEM was limited to about 10 μm, and it is concluded that the films are not tight from the fact that C is always present in the Auger spectra. The amount of C varies between evaporations and corresponds to a surface concentration between 4% and 25%, as judged from the metals Ir, Pt, Co, and Ni where there is no peak overlap.

The high pressure measurements are carried out with a mixture of 1% D_2 in H_2 at 1 bar total pressure. The sample was first kept in the high pressure cell at 1 bar and 200 °C for at least 1 h, the time needed to align the gas sampling device. The measurements were then carried out for decreasing temperatures with start at 200 °C. To safeguard against changes in the reaction rate due to, e.g., contamination or structural changes of the surfaces, the first measurement was repeated at the end of the series. The total exposure time in the high pressure cell varied between 4 h and 2 days, and no change in the reaction rate was observed during this time. Mass spectra of the gas close to the sample surface were measured occasionally. No indications of the formation of methane or other hydrocarbons were found.

After the high pressure experiment, the sample is transferred back to the main chamber for AES analysis, while kept at 150 °C. No contaminants other than C could be detected after the high pressure experiment. Frequently, but not always, the amount of C had increased after the high pressure measurements. In some cases, surface concentrations up to 35% were measured. The character of the carbon peaks is graphitic for those metals where there is no peak overlap. However, the presence of small amounts of carbide cannot be excluded due to the large graphite background.

The mass spectrometer signal obtained for a gas component, I_i, $i=H_2$, HD, D_2, does not only depend on the partial pressure of the gas in the high pressure cell p_i but is also dependent on the local absolute temperature at the quartz capillary leak T_c,

$$I_i = \chi_i \frac{p_i}{T_c^{\alpha}}, \tag{1}$$

where χ_i and α are calibration factors. Usually, $\alpha \approx 1$.[17] The mass spectrometer signals measured over the graphite surface well away from any metal spots, $I_{i,\mathrm{gr}}$, correspond to the composition of the gas fed to the high pressure cell, and are used for calibration of the H_2 and D_2 signals.[16] By performing background measurements for each temperature, Eq. (1) can be used to find the local pressures of H_2 and D_2 according to

$$p_i = \frac{I_i}{I_{i,\mathrm{gr}}} p_{i,\mathrm{gr}}, \quad i = \mathrm{H_2}, \mathrm{D_2}. \tag{2}$$

Here, $p_{i,\mathrm{gr}}$ is the partial pressure over the graphite surface. p_{HD} is calculated according to

$$p_{\mathrm{HD}} = \frac{I_{\mathrm{HD}} - I_{\mathrm{HD,gr}}}{I_{\mathrm{H_2,gr}} \gamma_{\mathrm{HD}}} p_{\mathrm{H_2,gr}}, \tag{3}$$

where

$$\gamma_{\mathrm{HD}} = \frac{\chi_{\mathrm{HD}}}{\chi_{\mathrm{H_2}}}.$$

γ_{HD} is determined by comparing the measured HD signals to calculated values for p_{HD}.[13]

III. CALCULATIONS

A simple model is used in order to describe the reaction rate as a function of the partial pressures at the catalytic surface.[13] It is assumed that the sticking probability S has the same value irrespective of whether the adsorbing molecule is H_2, HD, or D_2 and that it only depends on the total coverage on the surface. Since the experiments are made with only 1% D_2, the total coverage is assumed to equal that corresponding to 1 bar of pure H_2. With the exception of Cu, there are no clear indications of isotope effects in S in the literature for the metals of interest here, see Sec. V A. If necessary, isotope effects can be taken into account in the model.[13]

The local net rate of consumption for the species, R_i can be expressed as

$$R_i = F_i S - r_i, \quad i = \mathrm{H_2}, \mathrm{HD}, \mathrm{D_2}. \tag{4}$$

Here, r_i is the desorption rate of species i per macroscopic unit area and F_i the molecular flux,

$$F_i = \frac{p_i}{\sqrt{2\pi m_i k T}}, \quad i = \mathrm{H_2}, \mathrm{HD}, \mathrm{D_2}, \tag{5}$$

where m_i is the molecular mass of species i, k the Boltzmann constant, and T the absolute temperature. In steady state, the concentrations of the surface species are constant, which requires that

$$R_{\mathrm{H_2}} = R_{\mathrm{D_2}} = -\tfrac{1}{2} R_{\mathrm{HD}}. \tag{6}$$

It is furthermore assumed that the desorption rates fulfill

$$r_{\mathrm{HD}} = \sqrt{K_F r_{\mathrm{H_2}} r_{\mathrm{D_2}}}, \tag{7}$$

where the flux equilibrium constant K_F is defined by

$$K_F = \frac{(F_{\mathrm{HD}}^{\mathrm{eq}})^2}{F_{\mathrm{H_2}}^{\mathrm{eq}} F_{\mathrm{D_2}}^{\mathrm{eq}}}. \tag{8}$$

Here, F_i^{eq} is the molecular flux of species i at equilibrium in the gas mixture. Hence

$$K_F = K_g \frac{\sqrt{m_{\mathrm{H_2}} m_{\mathrm{D_2}}}}{m_{\mathrm{HD}}}, \tag{9}$$

where K_g is the equilibrium constant for the gas phase reaction

$$\mathrm{H_2} + \mathrm{D_2} \rightleftharpoons 2\mathrm{HD}. \tag{10}$$

Under the conditions of interest here, $K_F < 4$.[13]

Equation (7) is, e.g., fulfilled if the rates are proportional to the products of the coverages of H and D, θ_{H} and θ_{D}.

$$r_{ij} = k_{ij} \theta_i \theta_j, \quad i,j = \mathrm{H}, \mathrm{D}$$

and the k_{ij} are independent of the H/D ratio on the surface and chosen so that the r_{ij} fulfill Eq. (7). Rate constants k_{ij} derived from transition state theory fulfill this requirement.[13]

Under the assumptions mentioned previously, and for $K_F < 4$, the net rate of HD consumption R_{HD} can be expressed in terms of the F_i, K_F, and S,[13]

$$R_{\mathrm{HD}} = S\left(F_{\mathrm{HD}} - \sqrt{K_F} \sqrt{\frac{B^2}{4} - \frac{A^2}{4} + B\sqrt{G} + G} \right), \tag{11}$$

where

$$A = F_{\mathrm{D_2}} - F_{\mathrm{H_2}},$$

$$B = \frac{4F_0}{K_F - 4},$$

$$G = \frac{K_F^2 (F_{\mathrm{D_2}} - F_{\mathrm{H_2}})^2 + 4K_F (2F_{\mathrm{H_2}} + F_{\mathrm{HD}})(2F_{\mathrm{D_2}} + F_{\mathrm{HD}})}{4(K_F - 4)^2},$$

$$F_0 = F_{\mathrm{H_2}} + F_{\mathrm{D_2}} + F_{\mathrm{HD}}.$$

The influence of isotope effects in the desorption energies and prefactors is taken into account by the use of Eq. (7). The model is valid for coverage dependent desorption energies and prefactors, as long as they do not depend on the (small) variations in H/D ratio on the surface.[13]

The gas composition at the point of measurement (the tip of the capillary) is obtained from numerical calculations of the local gas velocity, temperature, and partial pressures inside the gas sampling device.[13,16] In these calculations, the rates of consumption on the catalytic surface of the three species are given by Eqs. (11) and (6).[13,16]

The influence of the sticking probability S on the calculated product and reactant pressures at the capillary leak for a

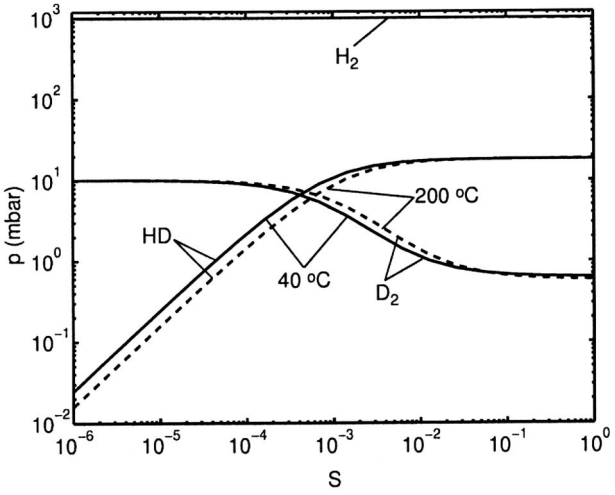

FIG. 2. The calculated partial pressures of H_2, HD, and D_2 at the capillary leak as a function of the sticking probability S at 40 (solid curves) and 200 °C (dashed curves). The gas mixture consists of 1% D_2 in H_2 at 1 bar total pressure and the flow rate is 100 $(ml/min)_n$. The capillary-surface distance Z_{cap} and the nozzle-surface distance Z_n are both 0.2 mm. The diameter of the metal spot is 1 mm.

certain set of parameters is shown in Fig. 2. In the low conversion region, the calculated partial pressure of HD at the leak is very close to being proportional to S. At higher conversion, there is a depletion in the minority reactant, D_2 in this case. For high values of S, the gas mixture at the surface is close to equilibrium and the reaction rate is limited by the transport rate for the different species in the gas phase. By interpolation in calculated curves such as the ones in Fig. 2, S can be determined from measured local partial pressures.

The lower detection limit for the HD pressure is determined by the sensitivity limit of the mass spectrometer, which is only 0.1 mbar in this case, due to the background of H_3^+ formed in the ion source.[13] From Fig. 2, 0.1 mbar corresponds to $S \approx 5 \times 10^{-6}$. For values of S where the reaction rate is determined by mass transport, only a minimum value for S can be obtained from the measured partial pressures. From Fig. 2, the maximum sticking probability which can be measured reliably is $S \approx 3 \times 10^{-2}$.

IV. RESULTS

A. Measured gas compositions

Figure 3 shows the partial pressure of D_2, p_{D_2}, and HD, p_{HD}, as a function of temperature when the gas sampling device is positioned 0.2 mm over the center of spots made of the various metals. The partial pressures p_{D_2} and p_{HD} were calculated from the measured ion currents with Eqs. (2) and (3), respectively. For comparison, data published earlier for Ni, Pd, and Pt have been included in the figure.[13] There was no significant decrease in the H_2 signal, and it is therefore not included in Fig. 3. The uncertainty in p_{D_2} is determined by the noise level of the mass spectrometer, which is about 1%. The dominating source of error when determining p_{HD} is the uncertainty in the distance between the sample and the gas sampling device, which is ±0.02 mm.[13] This deviation gives an uncertainty in p_{HD} of ±10%.[13]

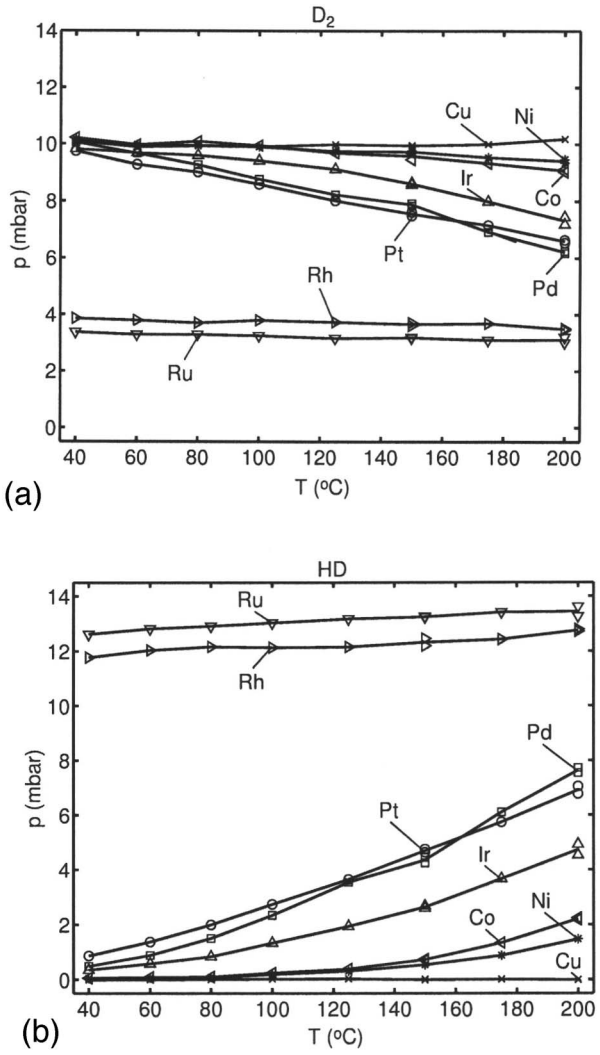

FIG. 3. Measured values for p_{D_2} (a) and p_{HD} (b) over the center of spots made of the different metals. The gas mixture consisted of 1% D_2 in H_2, i.e., the inlet partial pressure of D_2 is 10 mbars. The total pressure was 1 bar, and the flow rate 100 $(ml/min)_n$. For comparison, data for Ni, Pd, and Pt taken from Ref. 13 are included in the figure.

Qualitatively, p_{HD} increases with the H–D exchange rate. It is thus immediately clear that Ru is the most active of the metals for H–D exchange and that the activity for Rh and Ru is almost independent of temperature. Pt and Pd have comparable activity. The activity then decreases in the order Ir, Co, and Ni. No activity could be detected for Cu.

B. The sticking probability

The measured partial pressures are used to determine the sticking probability S by interpolation in diagrams such as those shown in Fig. 2. If the lowering in the D_2 pressure relative to the pressure over the graphite surface $p_{D_2,gr}$ is more than 8%, the measured D_2 pressure is used to determine S; else the HD pressure calculated from I_{HD} with Eq. (3) is used.

Figure 4 shows S as a function of temperature in all cases where the HD pressure was measurable. For Ru and Rh, S is above 1×10^{-3} and only weakly dependent on the temperature. Pt and Pd give comparable values for S, but the

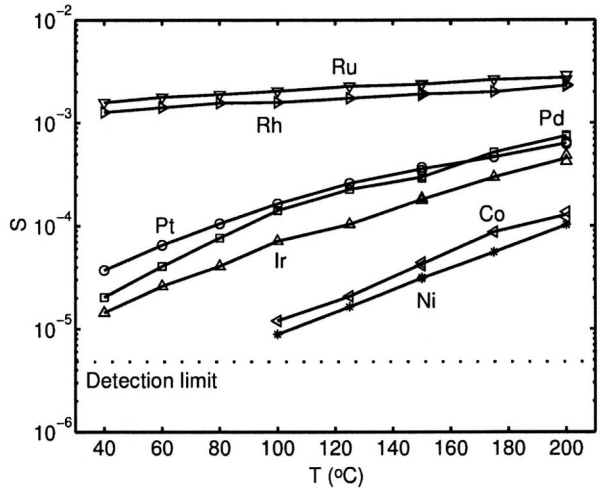

FIG. 4. Calculated sticking probabilities S for Co, Ni, Rh, Ru, Pd, Ir, and Pt in the temperature range 40–200 °C. The dotted line marks the lower detection limit for S. The signal for Cu is below the detection limit. The data for Ni, Pd, and Pt were taken from Ref. 13.

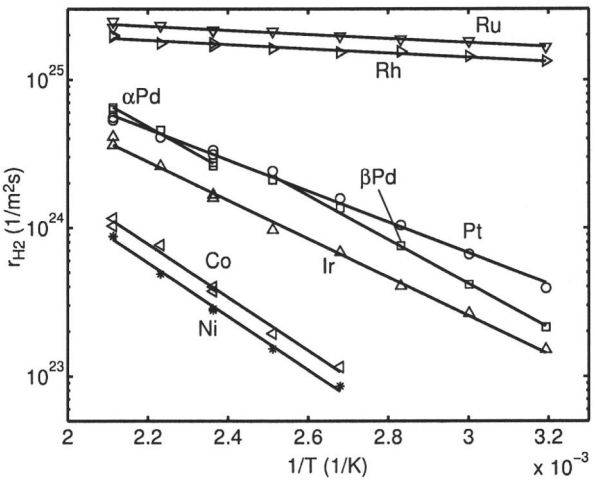

FIG. 5. Arrhenius plots of r_{H_2}. The plot for Pd is divided in one part below 150 °C, βPd, and one part above 150 °C, αPd (Ref. 13). The data for Ni, Pd, and Pt were taken from Ref. 13.

temperature dependence for Pd is slightly stronger than for Pt. The dip in the curve for Pd is ascribed to a phase transition between solid solution of H in Pd (αPd) and PdH (βPd) taking place at about 150 °C at 1 bar hydrogen pressure.[13,18] For the two least active metals, Co and Ni, S is only measurable above 80 °C. The data for Ni, Pd, and Pt were published previously.[13]

The shape of the curves for S as a function of T is very reproducible. However, there is a variation between different evaporations, so that the plots corresponding to the ones shown in Fig. 4 are offset relative to each other. The spread in the S values from the curves shown in Fig. 4 is about 50% for Ni, Pd, and Pt, see Ref. 13, and a factor of 2 for Rh and Ru. The reason for this is probably variations in the effective surface area, caused by, e.g., variations in the roughness of the substrate, due to repeated sputtering. As defined in the model, S is the sticking probability per unit area of the macroscopic surface. The reason for the larger variation for Ru and Rh is not known. However, the variation in S does not correlate with the amount of C determined by AES either before or after the high pressure experiment. The trend in S between the metals was established by direct comparison within the same experiment.

C. Apparent desorption energies for H_2

For a surface exposed to pure H_2 in steady state, the desorption rate, r_{H_2}, is equal to the adsorption rate,

$$r_{H_2} = SF_{H_2}. \tag{12}$$

It is instructive to calculate the apparent desorption energies[14] from data of how r_{H_2} depends on the temperature. The apparent desorption energy E_{app} is defined by assuming that r_{H_2} is given by the expression

$$r_{H_2} = \xi \exp\left(\frac{-E_{app}}{kT}\right), \tag{13}$$

where ξ is temperature independent. The apparent desorption energy may hence be obtained from a least squares adaption of the logarithm of Eq. (13) to an Arrhenius plot of r_{H_2}. Figure 5 shows typical Arrhenius plots. The average values and standard deviations for E_{app} and ξ extracted from the plots are displayed in Table I. No systematic curvature indicating a temperature dependent ξ could be detected in the Arrhenius plots.

In order to be able to compare the apparent desorption

TABLE I. Average values and standard deviations for E_{app} and ξ. The table also contains values for ν_{H_2} calculated from ξ with Eq. (14) under the assumption that the site density N_s is equal to the atomic density of the close-packed surface and that $\theta_H = 1$. For comparison, data for Ni, Pd, and Pt taken from Ref. 13 are included in the table. N is the number of measurements used to calculate E_{app} and ξ.

	E_{app} (kJ/mole H_2)	std (E_{app}) (kJ/mole H_2)	ξ ($m^{-2}\,s^{-1}$)	std (ξ) ($m^{-2}\,s^{-1}$)	N_s (m^{-2})	ν_{H_2} (s^{-1})	N
Ni	35	0.63	4×10^{27}	1×10^{27}	1.9×10^{19}	4×10^{8}	5
Co	34	⋯	6×10^{27}	⋯	1.5×10^{19}	8×10^{8}	1
Ru	2.4	0.19	6×10^{25}	2×10^{25}	1.6×10^{19}	4×10^{6}	4
Rh	3.2	0.66	6×10^{25}	5×10^{25}	1.6×10^{19}	4×10^{6}	4
βPd	29	1.9	1×10^{28}	6×10^{27}	1.5×10^{19}	1×10^{9}	9
Ir	24	1.5	1×10^{27}	1×10^{27}	1.6×10^{19}	6×10^{7}	2
Pt	21	1.4	1×10^{27}	6×10^{26}	1.5×10^{19}	1×10^{8}	9

energies E_{app} to calculated and measured values for the desorption energy E_{des}, it is assumed that the rate of desorption is given by the mean field expression

$$r_{H_2} = \frac{1}{2}\nu_{H_2}\theta_H^2 N_s \exp\left(\frac{-E_{des}}{kT}\right),$$

where N_s is the surface density of adsorption sites. It is assumed that the frequency factor ν_{H_2} is independent of T, according to common practice. In general, both ν_{H_2} and E_{des} are coverage dependent. However, provided that θ_H can be assumed to be constant over the range in T studied, it follows by comparison with Eq. (13) that E_{des} is comparable to E_{app} and that

$$\xi = \tfrac{1}{2}\nu_{H_2}\theta_H^2 N_s. \quad (14)$$

There seems to be no information available in the literature on θ_H as a function of the temperature at a hydrogen pressure of 1 bar. However, from the published isotherms for Pt(111), it seems reasonable that the hydrogen coverage is very close to 1 at temperatures below 200 °C and a hydrogen pressure of 1 bar.[5] Also, the low values obtained for the sticking probability indicate that the surface has a high coverage of H.[13] The reported initial binding energy for H on the other metals, with the exception of Cu, is higher than for Pt(111).[19–25] As a consequence, θ_H would be expected to be higher than for Pt. Hence, it is assumed that θ_H is approximately 1 over the temperature range studied for all the metals. The values for ν_{H_2} displayed in Table I were calculated from Eq. (14), under the assumptions that $\theta_H=1$ and that N_s equals the atomic density of the close-packed metal surfaces.

V. DISCUSSION

A. Sticking probabilities

Figure 6 shows the measured sticking probabilities S at 100 °C for all the metals investigated, with the exception of Cu. The figure also shows reported values for the sticking probability measured at high coverage under UHV conditions. The values plotted in Fig. 6 are those measured at the highest coverage obtained in each study. Table II contains a few comments to Fig. 6. In all the studies referenced, the sticking probability is found to decrease with increasing coverage. In some cases, S is reported to be well described by

$$S = S_0(1-\theta)^2, \quad (15)$$

where S_0 is the sticking probability at zero coverage and θ the hydrogen coverage.[12,28,32]

The values measured in this study are, in most cases, lower than those obtained under vacuum conditions. However, with the exception of Ni and Co, the trend in S between the metals seems to be roughly the same. The fact that S obtained in this study is lower than in the vacuum experiments can be explained by a higher hydrogen coverage. The hydrogen pressure of 1 bar used here is at least six orders of magnitude higher than in the vacuum experiments.

Adsorption of H_2 on Cu is activated. From isothermal uptake experiments on Cu(100), Rasmussen *et al.* report the barrier to be 48 and 56 kJ/mole for H_2 and D_2,

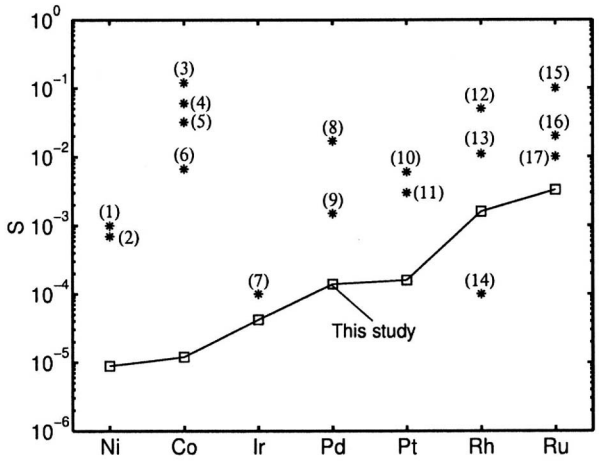

FIG. 6. Reported values for the sticking probability at high coverage and measured values for S at 100 °C. In the UHV experiments, adsorption was done with the gas at room temperature and the surface at the temperature T_s. The maximum coverage θ_{max} is 1 if nothing else is stated. (1) Ni(111), $\theta=0.99$, $T_s=140$ K (Ref. 26). (2) Ni(111), sputtered, $\theta=0.98$ (Ref. 11). (3) Polycrystalline Co, $\theta=0.88$, $T_s=195$ K (Ref. 19). (4) Co(10$\bar{1}$0), $\theta=1.14$, $T_s=200$ K (Ref. 20). (5) Polycrystalline Co, $\theta=1.1$, $T_s=78$ K (Ref. 27). (6) Co(0001), $\theta=0.12$, $T_s=300$ K (Ref. 21). (7) Ir(111), $\theta=0.8$, $T_s=100$ K (Ref. 28). (8) Pd(100), $\theta=1.3$, $T_s=170$ K (Ref. 29). (9) Pd(111), $\theta=1$, approximate, see Table II. (10) Pt(997), $\theta=0.7$, $T_s=120$ K (Ref. 30). (11) Pt(111), $\theta=0.7$, $T_s=120$ K (Ref. 30). (12) Rh(110), $\theta=1.7$, $T_s=85$ K, $\theta_{max}=2$ (Ref. 31). (13) Rh(111), $\theta=0.87$, $T_s=175$ K (Ref. 32). (14) Rh(111), $\theta=0.9$, $T_s=235$ K (Ref. 12). (15) Ru(10$\bar{1}$0), $\theta=1.6$, $T_s=100$ K, $\theta_{max}=2$ (Ref. 25). (16) Ru(0001), $\theta=1$, $T_s=100$ K (Ref. 33). (17) Ru(0001), $\theta=0.6$, $T_s=200$ K (Ref. 22).

respectively.[35] Extrapolation of the initial sticking coefficient S_0 using the value at 242 K obtained by Rasmussen *et al.* to determine the prefactor gives a value of 2.8×10^{-8} at 200 °C. Campbell and Campbell performed isothermal uptake experiments on oxygen covered Cu(110) at temperatures above 623 K.[36] If the reported activation energy and prefac-

TABLE II. Comments to Fig. 6.

(1) and (2)	Adsorption on Ni(111) is activated, but adsorption on defect sites and steps is unactivated (Ref. 11).
(3)	The sticking probability decreases with increasing temperature in the temperature range 195–298 K. θ is approximate as a consequence of surface roughness (Ref. 19).
(4)	Experiments made at 100 K give different results as a result of surface reconstruction (Ref. 20).
(5)	θ is approximate as a consequence of surface roughness (Ref. 27).
(7)	Adsorption follows Eq. (15) with $S_0=7.1\times10^{-3}$ (Ref. 28). S was calculated from the model.
(9)	The sticking probability at zero coverage was estimated to be 0.1–0.2 at room temperature (Ref. 34). Another study shows that S is independent of temperature in the range 325–425 K and that it drops at least a factor of 100 when the coverage increases to 1 (Ref. 9). This gives an approximate value of $S=1.5\times10^{-3}$.
(13)	Adsorption follows Eq. (15) with $S_0=0.65$ (Ref. 32). S was calculated from the model.
(14)	Adsorption follows Eq. (15) with $S_0=0.01$ (Ref. 12). S was calculated from the model.

tor are used to calculate a value at 200 °C, it is found that $S_0=2.87\times10^{-7}$. The extrapolated initial sticking coefficients thus indicate that the sticking probability should be below the sensitivity limit for the measurement of 5×10^{-6} for the clean Cu(110) and Cu(100) surfaces. Molecular beam experiments indicate that, in contrast to the situation for, e.g., Ni(111), the barrier is not affected by the presence of steps, defects, or impurities on the surface.[37] Thus, it is reasonable that adsorption on the polycrystalline surface studied here should be activated as well. In addition, at least for Cu(100), the sticking probability drops with increasing coverage.[35] Hence, it is not surprising that no activity can be measured for Cu in this experiment.

In the model, it is assumed that S is the same for H_2, HD, and D_2. This is not the case for Cu,[35] but since no activity could be measured for Cu, this is of no consequence here. For the other metals included in this study, there are very little experimental data on isotope effects in S or S_0. Thus, for Ni(111), the difference in S_0 between H_2 and D_2 at the temperatures of interest here is small or nonexistent.[38–41] A small isotope effect in S_0 has been reported for Pt(111).[42] From molecular beam experiments on Pt(111), however, it was concluded that there are no isotope effects in S_0.[43] For Ir(111) at 100 K and $\theta<0.8$, no difference in S between H_2 and D_2 is reported.[28] The same conclusion was reached for Pt(110) at 120 K and $\theta<0.8$.[28] Different values for S for H_2 and D_2 for $\theta>1$ on Rh(110) at 85 K were explained in terms of better long range order on the surface for adsorbed D.[31,44] It is questionable whether such effects are important at the temperatures of interest here.

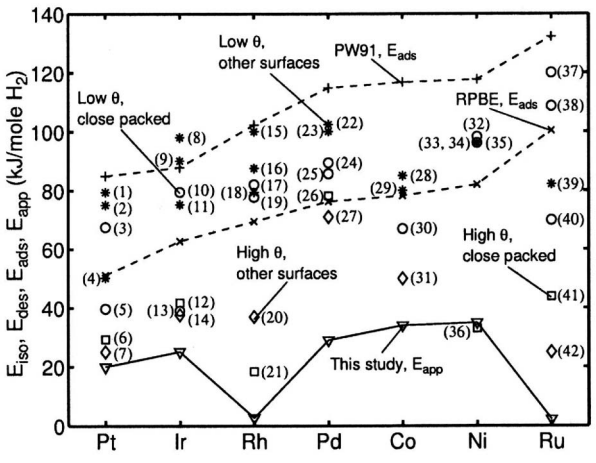

FIG. 7. Published values for the desorption energy E_{des}, the isosteric heat of adsorption E_{iso}, the calculated adsorption energy E_{ads}, and the apparent desorption energy E_{app} derived as part of this study. E_{ads} is shown both for the functionals PW91 and RPBE (Ref. 45). The maximum coverage θ_{max} is 1 if nothing else is stated. (1) E_{des}, Pt(110) (Ref. 28). (2) E_{iso}, Pt(111) terraces (Ref. 7). (3) E_{iso}, Pt(111) (Ref. 6). (4) E_{des}, Pt(997) (Ref. 30). (5) E_{iso}, E_{des}, Pt(111) (Ref. 5). (6) E_{iso}, Pt(111), $\theta=0.8$ (Ref. 5). (7) E_{iso}, Pt(997), $\theta=0.9$ (Ref. 30). (8) E_{des}, Ir(100) (Ref. 46). (9) E_{iso}, Ir(100) (Ref. 8). (10) E_{des}, Ir(111) (Ref. 28). (11) E_{des}, Ir(110) (Ref. 10). (12) E_{des} Ir(111), $\theta=0.4$ (Ref. 28). (13) E_{des}, Ir(111) (Ref. 47). (14) E_{des}, Ir(110), $\theta=0.7$ (Ref. 10). (15) E_{des}, Rh(100) (Ref. 48). (16) E_{iso}, Rh(110) (Ref. 31). (17) E_{des}, Rh(111) (Ref. 12). (18) E_{iso}, FEM tip (Ref. 49). (19) E_{des}, Rh(111) (Ref. 32). (20) E_{iso}, Rh(110), $\theta=1.2$, $\theta_{max}=2$ (Ref. 31). (21) E_{des}, Rh(111), $\theta=1$ (Ref. 32). (22) E_{iso}, Pd(100) (Ref. 29). (23) E_{iso}, Pd(110) (Ref. 34). (24) E_{des}, Pd(111) (Ref. 9). (25) E_{iso}, Pd(111) (Ref. 34). (26) E_{des}, Pd(111), $\theta=1$ (Ref. 9). (27) E_{iso}, Pd(100), $\theta=1.3$ (Ref. 29). (28) E_{iso}, evaporated film (Ref. 19). (29) E_{iso}, Co(10$\underline{1}$0) (Ref. 20). (30) E_{des}, Co(0001) (Ref. 21). (31) E_{iso}, evaporated film, $\theta=0.75$ (Ref. 19). (32) E_{iso}, Ni(111) (Ref. 26). (33) E_{iso}, Ni(111) (Ref. 4). (34) E_{iso}, Ni(100), Ni(110) (Ref. 4). (35) E_{des}, Ni(111) (Ref. 11). (36) E_{des}, Ni(111), $\theta=1$ (Ref. 11). (37) E_{des}, Ru(0001) (Ref. 23). (38) E_{des}, Ru(0001) (Ref. 24). (39) E_{iso}, E_{des}, Ru(10$\underline{1}$0) (Ref. 25). (40) E_{des}, Ru(0001) (Ref. 22). (41) E_{des}, Ru(0001), $\theta=0.8$ (Ref. 24). (42) E_{des}, Ru(10$\underline{1}$0), $\theta=1.7$, $\theta_{max}=2$ (Ref. 25).

B. The apparent desorption energy

Figure 7 shows E_{app} from Table I along with literature data for the heat of adsorption and the desorption energy for hydrogen on the metals of interest here, with the exception of Cu. A few comments regarding the studies cited in Fig. 7 are given in Table III. The experimental data included in Fig. 7 are the isosteric heat of adsorption E_{iso} derived from measured adsorption isotherms, and desorption energies E_{des} derived either from complete evaluation of TPD data or from molecular beam data, if nothing else is stated in Table III.

E_{iso} and E_{des} are only comparable if adsorption is unactivated, neglecting a term kT.[14] There is no indication of activated adsorption in the studies referenced in Fig. 7, except for the case of Ni(111).[11,26] Molecular beam experiments on Pt(111) at low hydrogen coverage have been interpreted in terms of activated adsorption.[54] However, later studies indicate that unactivated adsorption paths exist on the Pt(111) surface.[43,55] In principle, a significant barrier for adsorption could form as the coverage increases, even if adsorption is unactivated at low coverage. At least for Pt(111) up to a coverage of 0.4,[5] for Ru(10$\underline{1}$ 0) up to a coverage of 1.5,[25] and for Co(10$\underline{1}$ 0) up to a coverage of 0.5,[20] this does not seem to be the case, since the measured values for E_{des} are lower than those for E_{iso}. On Ni(111), where adsorption is activated at low coverage, the barrier for adsorption is lower than 0.4 kJ/mole H_2 for $\theta<0.9$.[26] In what follows, it will be assumed that adsorption is unactivated when comparing literature data for E_{iso} and E_{des} to E_{app}.

There are numerous theoretical calculations of the adsorption energy for hydrogen E_{ads} on the metals of interest in this study. In order to have calculations carried out in a consistent manner for all the metals, calculations made for 0.25 ML of H on the close-packed metal surfaces made with the functionals PW91 and RPBE have been plotted in Fig. 7.[45] The calculated values can be compared to the data for E_{iso} and E_{des} at low coverage on the close-packed surfaces. It is clear that there is a significant spread in the experimental data. However, most of the data points fall within the theoretical values obtained with PW91 and RPBE. Figure 7 also shows experimental data for other surfaces at low coverage, and it is clear that the difference between various surfaces at low coverage is not very significant. As a matter of fact, the values for E_{ads} calculated with the RPBE functional can be used as a reasonable descriptor for E_{des} at low coverage, independent of surface. It thus seems reasonable to let the calculations describe polycrystalline surfaces at low coverage too.

In general, the heat of adsorption and desorption ener-

TABLE III. Comments to Fig. 7.

(1) and (11)	E_{des} has a maximum at intermediate coverage for Ir(110) and Pt (110) (Refs. 10 and 28).
(9)	Unreconstructed (1×1) surface.
(14)	E_{des}=90 kJ/mole H_2 at θ=0.8 for Ir(100) (Ref. 46).
(21)	The TPD data were evaluated according to Chan, which means that E_{des} for $\theta>0$ is only an effective parameter (Ref. 32). The same evaluation method did, however, give good agreement with a complete evaluation of TPD data according to King in the case of Ni(111) (Ref. 11). On the other hand, the TPD data have also been explained with a model for adsorbate repulsion which gives a drop in E_{des} of only 15% when θ increases from 0 to 1 (Ref. 50).
(24) and (26)	E_{des} was derived under the assumption that S is described by Eq. (15) and that the frequency factor for desorption is independent of coverage (Ref. 9).
(27)	The fact that a coverage higher than 1 was achieved has been explained by absorption of H in the Pd bulk (Ref. 51).
(30)	From TPD experiments with adsorption at 300 K it was concluded that E_{des}=67 kJ/mole by fitting the data to a second order isotherm (Ref. 21). The maximum coverage obtained in the experiment is about 0.13. The authors note that this is the same maximum coverage as obtained in a similar study on Ni(111) at 298 K (Ref. 52). Thus, it seems reasonable that E_{des} for Co(0001) should be similar to E_{des} for Ni(111). This is also the conclusion from calculations made for a coverage of 0.25 (Ref. 45). Another theoretical study shows that Ni(111) and Co(0001) have almost identical binding energies for H at coverages of both 0.5 and 1 (Ref. 53).
(36)	The data for a surface with defects were chosen as being more relevant for the polycrystalline surfaces studied here. For a "perfect" Ni(111) surface, E_{des}=77 kJ/mole H_2 at θ=1 (Ref. 11).
(41)	Feulner and Menzel report that E_{des}=90 kJ/mole H_2 at θ=0.9 for Ru(0001) (Ref. 23). The value from Ref. 24 for θ=0.8 was used instead, since E_{des}=35 kJ/mole H_2 at θ=0.5 is found in Ref. 22.

gies derived from UHV experiments is found to decrease with coverage. However, there are less data available at high coverage, and in some cases there are large differences between different surfaces,[10,23,24,46] or even between studies on the same surface.[22–24] The close-packed (111) and (0001) surfaces can be expected to be representative for the majority of sites on the polycrystalline surfaces, and therefore data for the highest coverages investigated for those surfaces are shown in Fig. 7. On the other hand, other adsorption states with low desorption energy could dominate the adsorption/desorption process at high coverage. Hence, Fig. 7 also shows data for the other surfaces if the coverage investigated is higher and the energy lower than for the close-packed surface. In cases where large discrepancies between studies of the same surface exist in the literature, this is stated in Table III.

As can be seen from Fig. 7, the values for E_{app} found in this study are not much lower than literature data for E_{iso} and E_{des} obtained at high coverage. The exception is Pd, which is not unexpected, since it is difficult to obtain a high surface coverage of H on Pd under vacuum conditions due to the large solubility for H in the bulk. This is especially true for any sites with low adsorption energy.

The drop in the heat of adsorption (desorption energy) with coverage observed in the UHV experiments on the close-packed surfaces has frequently been explained by adsorbate-adsorbate repulsion.[29,31,56] The adsorption state with the lowest desorption energy is expected to dominate the overall desorption rate in the experiments carried out as part of this study. Provided that the defect sites on the polycrystalline surfaces studied here bind hydrogen stronger than the close-packed facets, the apparent desorption energy should be comparable to the desorption energy measured on a perfect single crystal surface.

Another explanation for the drop in desorption energy with coverage is that there is an ensemble of adsorption sites with varying desorption energy on the surface.[28] In this case, both E_{iso} and E_{des} obtained in the UHV experiments are effective values for all the sites available. The effective adsorption energy decreases with coverage because adsorption sites with successively lower desorption energy become populated as the coverage increases. Even the best single crystals contain a few percent of steps and defects. Less than 5% of defects on a Ni(111) surface was reported to change the desorption energy for θ=1 from 77 to 33 kJ/mole H_2, when E_{des} was derived by complete evaluation of TPD data.[11] Interestingly, it seems that the desorption energy measured on polycrystalline samples also drops with coverage in the same way as for the single crystal surfaces.[19,57,58] The apparent desorption energy obtained in this study is an effective value for all the different adsorption sites present on the surface. Hence, if the drop in adsorption energy is, at least partially, an ensemble effect, it is not surprising that the apparent desorption energy obtained here agrees reasonably well with data for E_{des} and E_{des} obtained under UHV conditions.

An observation which supports this explanation is that there is some disagreement between calculations and measurements regarding the coverage dependence of the heat of adsorption (desorption energy). Recent calculations performed for the close-packed surfaces of Ni, Co, Rh, Pd, Pt, and Cu show that the differential adsorption energy, which is the quantity to be compared with experimental data, goes through zero at a coverage of a full monolayer.[59] However, for lower coverages, the drop in adsorption energy with coverage is significantly smaller than is seen in most of the experiments on single crystals.[59] Other published calculations show little or no decrease in the integral binding energy when the hydrogen coverage increases to a full monolayer.[46,51,53,60,61] There are, however, also calculations which show a significant decrease (>10 kJ/mole H_2) in the integral binding energy for coverages below a full monolayer.[55,62–66]

C. Frequency factors

The frequency factors ν_{H_2} obtained from the Arrhenius plots under the assumption that Eq. (14) is valid and neglecting the temperature dependence of θ_H are many orders of magnitude lower than the value of 10^{13} s^{-1} expected from

transition state theory.[14,67] This could be the consequence of desorption mainly taking place from a very rare site on the surface. However, the size of the deviation from 10^{13} s^{-1} and the fact that the defect density on the surfaces is expected to be very high seem to contradict that explanation.

Measurements of ν_{H_2} as a function of coverage are rare in the literature. For Ru(0001), one study reports that the prefactor decreases from 3×10^{14} to 1×10^{14} s^{-1} as the relative coverage increases from 0 to 1,[23] whereas another study reports a drop from 10^{17} s^{-1} at zero coverage to 10^{9} s^{-1} at a coverage of 0.9.[24] For Ir(111), the prefactor is reported to decrease from 2×10^{12} to 2×10^{8} s^{-1} at a coverage of 0.4.[28] The frequency factor is found to be strongly covariant with the desorption energy for Ir(110). At low coverage ν_{H_2} is 3×10^{10} s^{-1}, it then goes through a maximum value of 1×10^{13} s^{-1} and drops to 1×10^{8} s^{-1} at a coverage of 0.7.[10] The situation is similar for Pt(110). Here, ν_{H_2} is 2×10^{11} s^{-1} at low coverage and at a coverage of 0.65. The maximum is a factor of 100 higher.[28] The effective frequency factor for Rh(111) obtained from evaluation of TPD data according to Chan drops from 2×10^{12} to 1×10^{3} s^{-1} when the coverage increases from 0 to 1.[32] However, in a later study the TPD data are explained by a model for the adsorbate-adsorbate repulsion which gives a nearly constant frequency factor.[50] In summary, there is a large spread in the small amount of data available, but it is not uncommon that the frequency factor at high coverage is many orders of magnitude lower than 10^{13} s^{-1}. Whether the drop in frequency factor with coverage seen in the UHV experiments is a real effect or an artifact due to the evaluation of the data is not clear. However, if the drop in frequency factor is due to ensemble effects, it is not surprising that the prefactors obtained in this study are low too, since the desorption rate is described by a single Arrhenius function, just as in the evaluation of TPD data.

D. Trends in the sticking probability between metals

The comparison between the apparent desorption energy and the desorption energies and heats of adsorption derived from UHV studies depends on a number of assumptions, e.g., that the surface is essentially covered with H under the conditions studied here. Therefore, a more qualitative comparison to the data reported in the literature is in place. In general, it could be expected that the sticking probability should drop with increasing coverage and that the coverage at a certain pressure and temperature should increase with the heat of adsorption. This does, however, not hold for the sticking probability under the conditions studied here. Figure 8 shows the sticking probability at 100 °C for all the metals except Cu as a function of the heat of adsorption E_{ads} on the close-packed surfaces calculated with the functional RPBE for a hydrogen coverage of 0.25.[45] It is obvious that E_{ads} at low coverage is not a good descriptor for the sticking probability under the conditions studied here. From Fig. 7, there is a reasonable correlation between the calculated values for E_{ads} at 0.25 ML and experimental values obtained at low coverage. Thus, the trend in Fig. 8 would have been similar if the experimental values for low coverage had been used to plot the data. The advantage with the calculated values in this case is that they were calculated in the same way for all the metals.

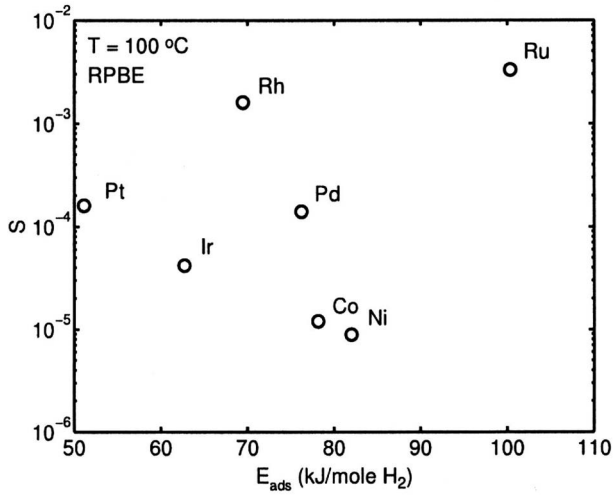

FIG. 8. The sticking probability S at 100 °C as a function of the adsorption energy E_{ads} calculated for 0.25 ML H with the functional RPBE taken from Ref. 45.

Surprisingly, the metal with the highest binding energy for H and Ru also gives the highest value for S. A possible explanation for this is that adsorption/desorption mainly occurs at sites with a low heat of adsorption, which are only populated at high hydrogen coverage. Hydrogen adsorption/desorption on Ru would then be an example of a system where the reaction rate is determined by the density of adsorption sites at the highest adsorption energy level populated, rather than by the adsorption energy at low coverage. Interestingly, the metals Rh, Ru, and Pd, which give higher values for S than would be expected from the adsorption energy, are all in the same row in the Periodic Table.

Another interesting observation is that there is a strong feature in the TPD curves obtained for Ru(11$\bar{2}$1) below 150 K.[68] The Ru(10$\bar{1}$0) surface shows a strong α state just above 200 K.[25,69] Similar features have also been reported for coadsorbed layers of H and CO on Ru(0001) and for surface alloys of Pt and Ru.[33,70] The TPD data for Ru(0001) show a single peak (and a shoulder) roughly between 300 and 400 K.[23,24,33,56,71] Similarly, the open Rh(110), Rh(100), and Rh(113) surfaces show a desorption feature at about 125 K.[31,48,50,72,73] A similar feature was also present in TPD curves on Rh(111), but was ascribed to defects or crystal edge sites.[32] This leads to the possibility that the extremely high activity for Ru and Rh observed here is somehow linked to the presence of steps, defects, or adsorbed C on the surface, since the presence of C on the surfaces cannot be ruled out in this experiment. It should, however, be mentioned that desorption features below 150 K in TPD data from Ir(100) and Ir(111) surfaces have been reported,[47,74] without Ir giving exceptionally high values for S in this experiment. With the exception for a desorption peak ascribed to hydrogen absorption in Pd bulk,[75] such features have not been ob-

served in any of the other studies referenced in this article, albeit the adsorption temperature was above 150 K in many cases.

E. Conclusions concerning PEM fuel cells

A few conclusions with respect to the PEM fuel cell may be drawn on the basis of this study, despite the fact that the system studied is very different from the anode catalyst in a PEM fuel cell under working conditions. First of all, unlike the situation for PEM fuel cells, Pt is not found to be the most effective of the pure metals when it comes to splitting hydrogen. It is, of course, possible that the mechanism for hydrogen splitting under working conditions in a PEM fuel cell is different from that for hydrogen splitting under the conditions studied here. However, it is also possible that the adsorption sites which give rise to the high sticking probability observed for Rh and Ru in this study are blocked by other adsorbates than H under operating conditions in a PEM fuel cell. As a matter of fact, during the course of this study, it was found that an air leak, giving rise to less than 1 ppm of oxygen in the D_2/H_2 mixture, completely deactivated Ru below 65 °C. At temperatures above 100 °C, the H–D exchange rate was identical to that in the pure D_2/H_2 mixture.

In contrast to what is found for the sticking probability in this study, the hydrogen evolution current in PEM fuel cells correlates well with the low coverage binding energy.[2] This is not in contradiction to the findings here since the mechanism for hydrogen evolution in solution is not necessarily the same as for hydrogen splitting in the gas phase.

The adsorption rate for Ru at 200 °C corresponds to a turnover frequency of approximately 2×10^6 s^{-1}. This corresponds to 450 A/cm^2 of catalytic metal area, and is several orders of magnitude higher than what is typically reached with a Pt anode catalyst in a PEM fuel cell. Hence, if there was a proton conduction membrane which could operate without water, the current density on the anode could be orders of magnitude larger than in the present day PEM fuel cells.

VI. SUMMARY

The sticking probability S for hydrogen at 1 bar is found to increase in the order Ni, Co, Ir, Pd, Pt, Rh, and Ru at temperatures below 150 °C. At higher temperatures, Pd gives higher values for S than Pt. The sticking probability for Cu is below the detection limit of the measurement. The values for S obtained in this study are lower than values measured at high hydrogen coverage under vacuum conditions. This could be a consequence of the higher coverage obtained in this study. The apparent desorption energies obtained in this study agree reasonably well with heats of adsorption and desorption energies measured at high coverage under vacuum conditions. However, the sticking probability, or equivalently, the adsorption/desorption rate for H_2, does not correlate with the adsorption energy at low coverage. In particular, the desorption rate for Ru and Rh is unexpectedly high, with an apparent energy for desorption which is only a few kJ/mole H_2. This is explained by the presence of adsorption states with low adsorption energy, possibly located at defects, which are only populated at high pressure. Hydrogen splitting/association on these metals at 1 bar is thus an example of a system where the density of adsorption states as a function of adsorption energy determines the reactivity, rather than the adsorption energy at low coverage.

ACKNOWLEDGMENTS

The Danish Research Council is gratefully acknowledged for funding the project "Towards a Hydrogen Society." Center for Individual Nanoparticle Functionality (CINF) is sponsored by The Danish National Research Foundation.

[1] J. Greeley and M. Mavrikakis, Nat. Mater. **3**, 810 (2004).
[2] J. K. Nørskov, T. Bligaard, A. Logadottir, J. R. Kitchin, J. G. Chen, S. Pandelov, and U. Stimming, J. Electrochem. Soc. **152**, J23 (2005).
[3] K. Christmann, Surf. Sci. Rep. **9**, 1 (1988).
[4] K. Christmann, O. Schober, G. Ertl, and M. Neumann, J. Chem. Phys. **60**, 4528 (1974).
[5] K. Christmann, G. Ertl, and T. Pignet, Surf. Sci. **54**, 365 (1976).
[6] P. R. Norton, J. A. Davies, and T. E. Jackman, Surf. Sci. **121**, 103 (1982).
[7] B. J. J. Koeleman, S. T. de Zwart, A. L. Boers, B. Poelsema, and L. K. Verhey, Nucl. Instrum. Methods Phys. Res. **218**, 225 (1983).
[8] T. Ali, A. V. Walker, B. Klötzer, and D. A. King, Surf. Sci. **414**, 304 (1998).
[9] T. Engel and H. Kuipers, Surf. Sci. **90**, 162 (1979).
[10] D. E. Ibbotson, T. S. Wittrig, and W. H. Weinberg, J. Chem. Phys. **72**, 4885 (1980).
[11] K. D. Rendulic and A. Winkler, Int. J. Mod. Phys. B **3**, 941 (1989).
[12] J. I. Colonell, T. J. Curtiss, and S. J. Sibener, Surf. Sci. **366**, 19 (1996).
[13] M. Johansson, O. Lytken, and I. Chorkendorff, Top. Catal. **46**, 175 (2007).
[14] I. Chorkendorff and J. W. Niemantsverdriet, *Concepts of Modern Catalysis* (Wiley, Weinheim, 2003).
[15] M. Johansson, J. Hoffmann Jørgensen, and I. Chorkendorff, Rev. Sci. Instrum. **75**, 2082 (2004).
[16] M. Johansson, T. Johannesen, J. Hoffman Jørgensen, and I. Chorkendorff, Appl. Surf. Sci. **252**, 3673 (2006).
[17] M. Johansson, I. Lundström, and L.-G. Ekedahl, Rev. Sci. Instrum. **71**, 3513 (2000).
[18] H. Frieske and E. Wicke, Ber. Bunsenges. Phys. Chem. **77**, 50 (1973).
[19] W. Lisowski, Appl. Surf. Sci. **35**, 399 (1988).
[20] K.-H. Ernst, E. Schwarz, and K. Christmann, J. Chem. Phys. **101**, 5388 (1994).
[21] M. E. Bridge, C. M. Comrie, and R. M. Lambert, J. Catal. **58**, 28 (1979).
[22] H. Shimizu, K. Christmann, and G. Ertl, J. Catal. **61**, 412 (1980).
[23] P. Feulner and D. Menzel, Surf. Sci. **154**, 465 (1985).
[24] J. A. Schwarz, Surf. Sci. **87**, 525 (1979).
[25] G. Lauth, E. Schwarz, and K. Christmann, J. Chem. Phys. **91**, 3729 (1989).
[26] K. D. Rendulic and A. Winkler, J. Chem. Phys. **79**, 5151 (1983).
[27] W. Lisowski, Appl. Surf. Sci. **37**, 272 (1989).
[28] J. R. Engstrom, W. Tsai, and W. H. Weinberg, J. Chem. Phys. **87**, 3104 (1987).
[29] R. J. Behm, K. Christmann, and G. Ertl, Surf. Sci. **99**, 320 (1980).
[30] K. Christmann and G. Ertl, Surf. Sci. **60**, 365 (1976).
[31] M. Ehsasi and K. Christmann, Surf. Sci. **194**, 172 (1988).
[32] J. T. Yates, Jr., P. A. Thiel, and W. H. Weinberg, Surf. Sci. **84**, 427 (1979).
[33] T. Diemant, T. Hager, H. E. Hoster, H. Rauscher, and R. J. Behm, Surf. Sci. **541**, 137 (2003).
[34] H. Conrad, G. Ertl, and E. E. Latta, Surf. Sci. **41**, 435 (1974).
[35] P. B. Rasmussen, P. M. Holmblad, H. Christoffersen, P. A. Taylor, and I. Chorkendorff, Surf. Sci. **287/288**, 79 (1993).
[36] J. M. Campbell and C. T. Campbell, Surf. Sci. **259**, 1 (1991).
[37] G. Anger, A. Winkler, and K. D. Rendulic, Surf. Sci. **220**, 1 (1989).
[38] J. N. Russel, Jr., S. M. Gates, and J. T. Yates, Jr., J. Chem. Phys. **85**, 6792 (1986).
[39] J. T. Yates, Jr., J. N. Russel, Jr., I. Chorkendorff, and S. M. Gates, in *Kinetics of interface reactions*, Springer Series in Surface Science Vol. 8,

edited by M. Grunze and H. J. Kreuzer (Springer-Verlag, Heidelberg, 1987).
[40] H. P. Steinrück, M. Luger, A. Winkler, and K. D. Rendulic, Phys. Rev. B **32**, 5032 (1985).
[41] D. O. Hayward and A. O. Taylor, Chem. Phys. Lett. **124**, 264 (1986).
[42] E. G. Seebauer, A. C. F. Kong, and L. D. Schmidt, Surf. Sci. **176**, 134 (1986).
[43] A. C. Luntz, J. K. Brown, and M. D. Williams, J. Chem. Phys. **93**, 5240 (1990).
[44] K. Christmann and M. Ehsasi, Appl. Phys. A: Solids Surf. **44**, 87 (1987).
[45] J. Greeley and M. Mavrikakis, J. Phys. Chem. B **109**, 3460 (2005).
[46] D. Lerch, A. Klein, A. Schmidt, S. Müller, L. Hammer, K. Heinz, and M. Weinert, Phys. Rev. B **73**, 075430 (2006).
[47] K. Moritani, M. Okada, M. Nakamura, T. Kasai, and Y. Murata, J. Chem. Phys. **115**, 9947 (2001).
[48] L. J. Richter and W. Ho, J. Vac. Sci. Technol. A **5**, 453 (1987).
[49] V. V. Gorodetskii, B. E. Nieuwenhuys, W. M. H. Sachtler, and G. K. Boreskov, Surf. Sci. **108**, 225 (1981).
[50] S. H. Payne, H. J. Kreuzer, W. Frie, L. Hammer, and K. Heinz, Surf. Sci. **421**, 279 (1999).
[51] S. Wilke, D. Hennig, R. Löber, M. Methfessel, and M. Scheffler, Surf. Sci. **307–309**, 76 (1994).
[52] J. Lapujoulade and K. S. Neil, J. Chem. Phys. **57**, 3535 (1972).
[53] D. J. Klinke II and L. J. Broadbelt, Surf. Sci. **429**, 169 (1999).
[54] M. Salmeron, R. J. Gale, and G. A. Somorjai, J. Chem. Phys. **70**, 2807 (1979).
[55] R. A. Olsen, G. J. Kroes, and E. J. Baerends, J. Chem. Phys. **111**, 11155 (1999).
[56] K. L. Kostov, W. Widdra, and D. Menzel, Surf. Sci. **560**, 130 (2004).
[57] G. Wedler, F. J. Bröcker, G. Fisch, and G. Schroll, Z. Phys. Chem., Neue Folge **76**, 212 (1971).
[58] A. Crucq, G. Lienard, L. Degols, and A. Frennet, Appl. Surf. Sci. **17**, 79 (1983).
[59] G. Karlberg and E. Skulason, personal communication.
[60] P. Legare, Surf. Sci. **559**, 169 (2004).
[61] I. M. Ciobica, A. W. Kleyn, and R. A. Van Santer, J. Phys. Chem. B **107**, 164 (2003).
[62] J.-F. Paul and P. Sautet, Phys. Rev. B **53**, 8015 (1996).
[63] O. M. Løvvik and R. A. Olsen, Phys. Rev. B **58**, 10890 (1998).
[64] R. Löber and D. Hennig, Phys. Rev. B **55**, 4761 (1997).
[65] Z. Ke, W. Lai, and D. Xie, J. Appl. Phys. **99**, 113704 (2006).
[66] J. Greeley and M. Mavrikakis, Surf. Sci. **540**, 215 (2003).
[67] R. I. Masel, *Principles of Adsorption and Reaction on Solid Surfaces* (Wiley, New York, 1996).
[68] C. Y. Fan and K. Jacobi, Surf. Sci. **482–485**, 21 (2001).
[69] P. Lenz and K. Christmann, J. Catal. **139**, 611 (1993).
[70] D. E. Peebles, J. A. Schreifels, and J. M. White, Surf. Sci. **116**, 117 (1982).
[71] J. T. Yates, Jr., C. H. F. Peden, J. E. Houston, and D. W. Goodman, Surf. Sci. **160**, 37 (1985).
[72] K. Christmann, M. Ehsasi, W. Hirschwald, and J. H. Block, Chem. Phys. Lett. **131**, 192 (1986).
[73] W. Nichtl-Pecher, W. Stammler, K. Heinz, and K. Müller, Phys. Rev. B **43**, 6946 (1991).
[74] K. Moritani, M. Okada, T. Kasai, and Y. Murata, Surf. Sci. **445**, 315 (2000).
[75] U. Muschiol, P. K. Schmidt, and K. Christmann, Surf. Sci. **395**, 182 (1998).